
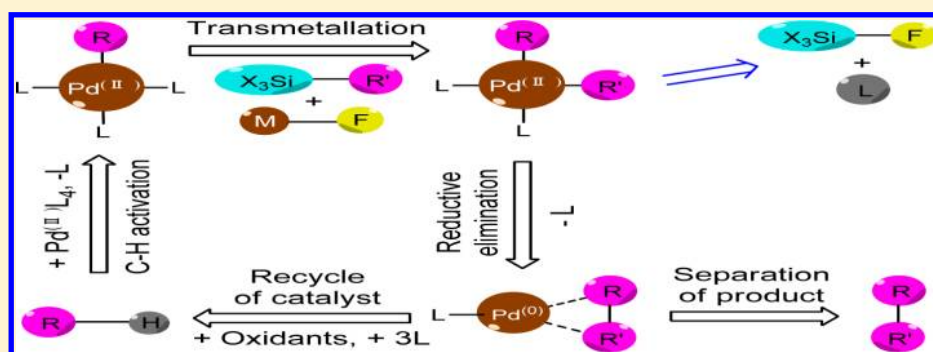


# Catalytic C–H Activation/C–C Coupling Reaction: DFT Studies on the Mechanism, Solvent Effect, and Role of Additive

Lei Zhang and De-Cai Fang\*

Key Laboratory of Theoretical and Computational Photochemistry, Ministry of Education, College of Chemistry, Beijing Normal University, Beijing 100875, China

 Supporting Information



**ABSTRACT:** A series of density functional theory (DFT) experiments, employing the B3LYP+IDSCRF/BS1 and B3LYP+IDSCRF/DZVP methods, have been carried out for the  $\text{Pd}(\text{OAc})_2$ -catalyzed enamide–siloxane C–H activation/C–C coupling reactions. The results reveal that there are four processes, namely C–H activation, transmetalation (TM), reductive elimination (RE), and separation of product (SP) and recycling of catalyst (RC), each of which is consist of different steps. In order to fully understand the origin of regiospecific C–H activation/C–C coupling on the alicyclic ring experimentally observed, the conformational preference, kinetic aspects, and relative stabilities of the competitive products have been explored. In addition, the roles of additive silver salt  $\text{AgF}$  and solvent dioxane have also been addressed, providing valuable details upon which to rationally optimize experimental conditions.

## 1. INTRODUCTION

Reactions forming new C–Y bonds ( $Y = \text{C}, \text{N}, \text{O}$ , etc.) are of high value for synthetic and industrial chemists. The traditional method involves the conversion of a substrate C–H bond to a C–X bond ( $X = \text{Cl}, \text{Br}, \text{I}$ , etc.), followed by reaction with C-, N-, or O-containing nucleophiles.<sup>1</sup> The importance of hydrocarbylation and carbon chain growth have resulted in a similar and concurrent explosion in research focus on C–C cross-coupling reactions, with particular attention to reactions of haloalkanes with organometallic reagents. Of note are the Suzuki–Miyaura,<sup>2</sup> Negishi,<sup>3</sup> Migita–Kosugi–Stille,<sup>4</sup> and Hiya–ma couplings.<sup>5</sup> Each of these share the common feature of the new C–C bond being formed by catalytic Pd or Ni complexes and organometallic compounds as coupling partners, to react with the substrate C–X bond. A shared disadvantage for these types of reactions is that the organohalogen compounds must be prepared via halogenation reactions for the oxidative addition, resulting in poor atom economy and overall nongreen chemistry.<sup>6</sup>

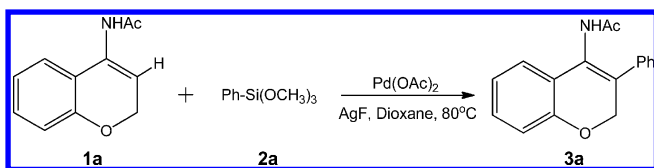
Since 2000, a more straightforward and economical method, activating the C–H bond using palladium(II) catalysts or some other transition-metal complexes, has been developed and refined.<sup>7</sup> Numerous works in the literature address the formation of C–C,<sup>7a–d</sup> C–N,<sup>7e,f</sup> and C–O<sup>7g–i</sup> bonds via direct

C–H activation, employing organoboron,<sup>8</sup> organotin,<sup>9</sup> organosilicon,<sup>10</sup> and organozinc.<sup>11</sup> Organoboron agents have been especially well developed and widely used for C–H activation/C–C coupling reactions, while the other three related reactions are still under development.

Because of the exponential growth of C–H activation reactions and their importance to C–C bond construction, a number of experimental<sup>12a–f</sup> and theoretical<sup>12g–m</sup> studies were conducted to resolve the mechanisms involved in the breaking of the C–H bond and the role of the catalytic species.<sup>12</sup> The common acceptable mechanism known as proton-abstraction<sup>12c</sup> involves the hydrogen atom of the C–H bond being abstracted by one of the  $\text{Pd}(\text{OAc})_2$  acetate ligands, generating the corresponding six-membered cyclic transition state. Experimental<sup>13a–c</sup> and theoretical<sup>13d,e</sup> works suggest that transmetalation (TM) with organosilicons could be accelerated with the existence of  $\text{F}^-$ . In 2009, Zhou and co-workers<sup>10c</sup> reported a cross-coupling reaction of cyclic enamide **1a** and trimethoxyphenylsilane **2a** via  $\text{sp}^2$  C–H activation by catalytic  $\text{Pd}(\text{OAc})_2$  (Scheme 1). Only C–C cross-coupling on the alicyclic ring was observed, an example of regiospecific C–H

**Received:** November 28, 2012

**Scheme 1. Pd(OAc)<sub>2</sub>-Catalyzed C–H Activation/C–C Cross-Coupling Reaction of an Enamide (1a) and an Aryl Siloxane (2a) Characterized in This Work by DFT Experiments**



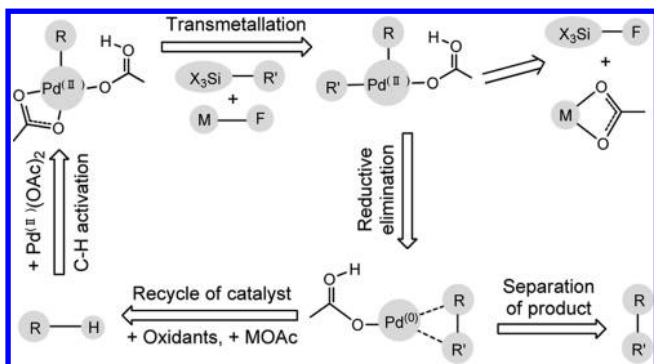
activation. This work screened fluoride sources and solvents, showing 3 equiv of AgF under dioxane generated the desired coupling product in high yield, while toluene and 1,2-dichloroethane (DCE), despite having similar dielectric constants as dioxane, resulted in poor yield of product (<50%). However, the greatest shortcoming is that there is no rational explanation of these observations.

Considering the importance and versatility of C–C cross-coupling reactions via direct C–H activation, it is imperative to develop mechanistic understanding of these reactions. Theoretical studies have previously focused on individual processes, rather than the entire catalyzed reaction cycle,<sup>12m</sup> until now. We therefore carried out a series of density functional theory (DFT) experiments to quantitatively characterize the structural and energetic aspects of a C–H activation/C–C cross-coupling reaction of a cyclic enamide **1a** and an aryl siloxane **2a** (Scheme 1). The results of these DFT experiments, including the location of all possible stationary points along their respective reaction pathways, energy and free energy profiles, solvent effects and the role of additive AgF are presented herein. It is our belief that this extensive investigation provides valuable details upon which to rationally optimize experimental conditions.

## 2. RESULTS AND DISCUSSION

Catalytic cycles of C–H activation/C–C cross-coupling reactions with organometallic partners are traditionally separated into the following steps: C–H activation, transmetalation (TM), reductive elimination (RE), the separation of product (SP) and recycling of catalyst (RC) (Scheme 2). In reality, the mechanism is not so simple, as other mechanistic stages accompany each of these five steps and are detailed in the following sections. For simplicity, the reported results are

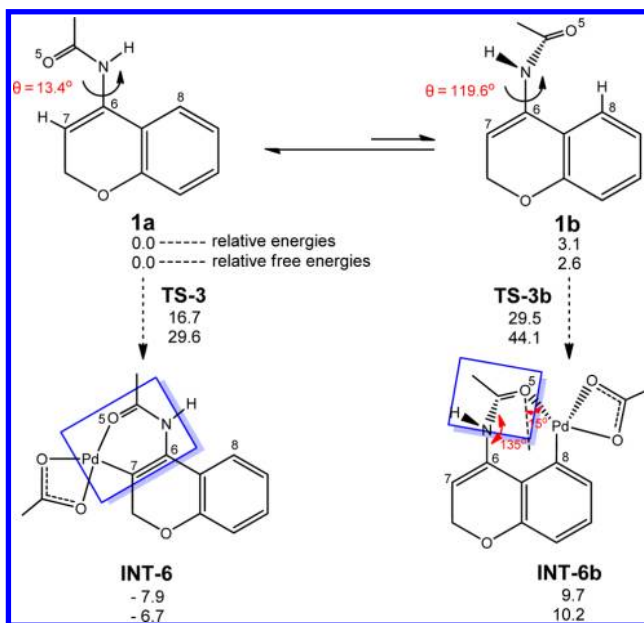
**Scheme 2. Schematic Depiction of the Entire Catalyzed Cycle for C–H Activation/C–C Cross-Coupling Reaction with Organosilicon Partners**



based on B3LYP+IDSCRF/DZVP calculations, except as noted elsewhere.

**2.1. Reaction Mechanisms.** Rotation about the enamide C6–N bond [C(O5)–N–C6–C7] affords two possible stable conformers with dihedral angles of 13.4° (**1a**) and 119.6° (**1b**) (Scheme 3). The energies and free energies of **1a** are 3.1 and

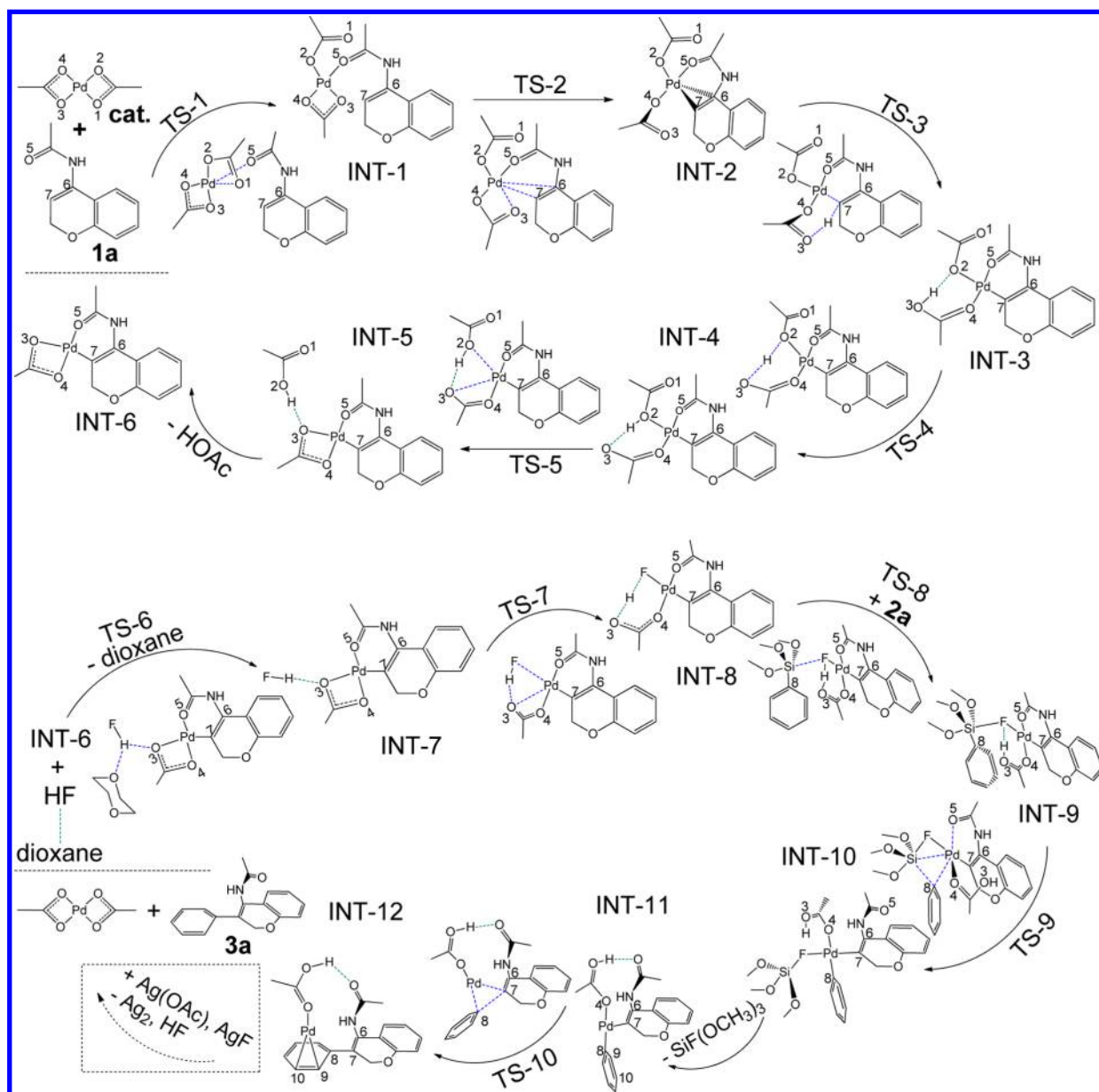
**Scheme 3. Geometric Representations of the Two Stable Conformers and Their Corresponding C–H Activation Processes, along with Their Relative Energies (ΔE) and Free Energies (ΔG) (kcal/mol)**



2.5 kcal/mol lower than those of **1b**, respectively, indicating that the predominant orientation of the carbonyl group in **1a** influences regio-selective C–H activation at the C7-atom on the alicyclic ring experimentally observed. Specifically, that the geometry of the reactant–catalyst coordination places the C7–H bond in relatively close proximity to the Pd center, with respect to the other C–H bonds. This is in good agreement with the complex-induced proximity effect (CIPE) proposed by Beak and Snieckus.<sup>7n</sup> Based on this finding, the C–H activation mechanisms involving enamide **1a** were considered in the beginning.

Optimized geometric structure for the stationary points located along the reaction profiles are shown in Figure 1, along with the atomic numbering used. The reaction begins with enamide **1a** binding the Pd(OAc)<sub>2</sub> catalyst through a five-coordinate transition state (TS-1), subsequently relaxing to a four-coordinate square intermediate (INT-1). From the structure of TS-1, it is observed that as the O5 of the substrate carbonyl group attacks the Pd center, concomitant with departure of the O1 atom from one of the η<sup>2</sup>-ligated-CH<sub>3</sub>COO<sup>−</sup> groups, freeing space for the approach of the O5 atom; leading to a η<sup>2</sup> → η<sup>1</sup> hapticity change in the CH<sub>3</sub>COO<sup>−</sup> ligand in INT-1.

The substrate C6–C7 double bond subsequently replaces the other η<sup>2</sup>-CH<sub>3</sub>COO<sup>−</sup> ligand to form INT-2 via the TS-2 transition state. This is accompanied by a slight lengthening of interatomic distances in TS-2 as follows: Pd–C6, Pd–C7, and Pd–O3 are 2.83, 2.68, and 2.68 Å, respectively, about 0.52, 0.43, and 0.54 Å longer than those in INT-2 (Pd–C) or INT-1



**Figure 1.** Geometrical structures of all stationary points along the reaction pathway in which the partially formed or cleaved bonds in transition states and weak interatomic interactions are represented by dashed lines.

(Pd–O). Following this, the cleavage of the C7–H bond and the  $\text{CH}_3\text{COO}^-$ -induced hydrogen transfer within the ligand field proceed in a concerted manner via a six-membered ring transition state (TS-3), with the bond lengths of Pd–C7, H–C7, and H–O3 being 2.13, 1.31, and 1.36 Å, respectively. The intermediate formed (INT-3) is feathered by a Pd-containing six-membered ring structure, and involves an intramolecular hydrogen-bond ( $\text{O3}\cdots\text{H}\cdots\text{O2}$ ), facilitating an intramolecular hydrogen transfer via the TS-4 structure to form a new intermediate (INT-4), itself displaying a stabilizing  $\text{O3}\cdots\text{H}\cdots\text{O2}$  H-bond. An intramolecular substitution or  $\eta^1\text{-CH}_3\text{COO}^-$  cyclization displaces a neutral acetic acid, generating intermediate INT-5, bearing one  $\eta^2\text{-CH}_3\text{COO}^-$  in the ligand field. The final step in the C–H activation process to attain intermediate INT-6 is accomplished by direct removal of the neutral acetic acid from INT-5 without any transition state.

Although the cyclopalladation intermediate (INT-6) is favored by the predominant orientation of the carbonyl group

in 1a based on the CIPE model, the possibility of C–H activated at ortho-position on the aromatic ring via seven-membered cyclopalladation should also be considered. Comparing the possible reaction route 1a  $\rightarrow$  INT-6 with that of 1b  $\rightarrow$  INT-6b in Scheme 3, one can realize that the former is obviously more favorable than the latter both dynamically and thermodynamically: (a) The free energy of 1a is about 2.6 kcal/mol lower than that of 1b, indicating that the concentration of 1a should be larger than that of 1b if they are in the state of equilibrium. (b) The activation barrier for rate-controlling step of the former is about 9.7 kcal/mol lower than that of latter. (c) The process of the 1a  $\rightarrow$  INT-6 is exothermic, while that of 1b  $\rightarrow$  INT-6b is endothermic. These results might be related to geometric parameters of 1b, TS-3b, and INT-6b, for example, the carbonyl group in 1b is obviously apart from the mainframe in order to avoid the repulsion between O5 and hydrogen of C8, leading to the dihedral angle between mainframe and carbonyl group being  $119.6^\circ$ . The geometric parameters in

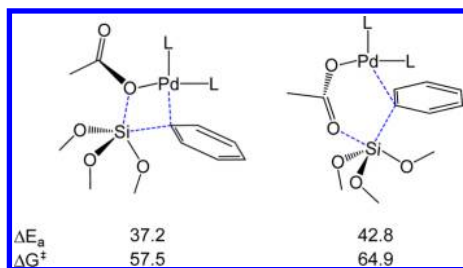


**INT-6b** indicate that the Pd–O5 bond axis deviates from the carbonyl plane by 21° and the C(O5)–N–C6 bond angle is about 135°, substantially larger than a normal angle (~120°) (i.e., the seven-membered ring is too strained). The details are available in the Supporting Information.

The acetic acid CH<sub>3</sub>COOH molecule generated in the C–H activation process is able to react with one molecule of AgF with the help of a dioxane solvent molecule [CH<sub>3</sub>COOH + AgF + dioxane → HF···dioxane + Ag( $\eta^2$ -OAc)] and is shown to be a spontaneous process ( $\Delta G = -6.4$  kcal/mol); details of this process are discussed in the Results and Discussion. The intermolecularly H-bonded HF···dioxane complex generated aids to accelerate the TM process. First, the HF molecule is transferred from dioxane to the O3-atom in the arm of the  $\eta^2$ -CH<sub>3</sub>COO<sup>−</sup> ligand in **INT-6**, leading to an intermediate (**INT-7**) with a very tight H-bond (F–H···O = 1.58 Å), facilitating release of a dioxane molecule back into solution. This leads to formation of **INT-8** through replacement of O3 by the F-atom from HF, mediated by a four-center transition structure (**TS-7**), in which a strong and nearly symmetrical O···H···F H-bond is formed. This is followed by the F-atom in **INT-8** attack the Si-atom in Si(OCH<sub>3</sub>)<sub>3</sub>Ph to form an intermediate (**INT-9**) through the **TS-8** transition state, wherein the distance of Si–F is only 2.02 Å or ~0.06 Å longer than that in the free pentavalent SiF(OCH<sub>3</sub>)<sub>3</sub>Ph<sup>−</sup> species. The transfer of the phenyl ring to the Pd-atom from the Si-atom passes through transition state **TS-9**, in which the Si-atom and the Ph-ring approach the Pd center, pushing the oxygen carbonyl O5-atom away from Pd, forming intermediate **INT-10**. Therein, the Si- and Pd-atoms are separated and form a near-planar four-coordinate Pd structure, very stable Pd(II).

We have also located two possible TM paths in the absence of an HF molecule, as depicted in Scheme 4. Such four-

**Scheme 4. Transition Structures for TM Mechanisms in the Absence of an HF Molecule, along with Their Relative Activation Energies ( $\Delta E_a$ ) and Free Energies ( $\Delta G^\ddagger$ ) (kcal/mol)**



membered and six-membered transition states are not favorable both in energy and free energy with respect to the HF-assisted pathway; comparative information is detailed in the Supporting Information.

Direct rupture of the SiF(OCH<sub>3</sub>)<sub>3</sub> moiety from **INT-10** should proceed easily, reflected by the loose Pd←F coordinating bond (2.55 Å) and serious steric congestion. It can be observed that the T-shape three-coordinate intermediate (**INT-11**) formed has proven to be a more reactive precursor for C–C bond coupling with respect to the four-coordinate intermediate (**INT-10**), with the energy barrier of RE process from **INT-11** being 5.1 kcal/mol lower than that from **INT-10**. Such a conclusion is in good agreement with the related theoretical works reported recently.<sup>14</sup> The Pd–C bonds in

**INT-11** are in the ortho-position, which is favorable for RE to form **INT-12** via **TS-10** transition state, concurrently changing the oxidation state of Pd to zero [Pd(II) → Pd(0)].

The RE step ends at **INT-12**, in which the product **3a** cannot be directly removed, since there are two strong Pd→C coordinating bonds. Therefore, in order to recover the Pd(OAc)<sub>2</sub> catalyst, Pd(0) should be oxidized to Pd(II), hence the requisite AgF and Ag(OAc) salts. The molecular roles of the AgF and Ag(OAc) are to remove an H-atom from CH<sub>3</sub>COOH and to provide a second CH<sub>3</sub>COO<sup>−</sup> anion for coordination to the Pd-center. The oxidation involves a complicated, multistep and multichannel process, addressed in section 2.2.

The relative energy and free energy profiles are depicted in Figure 2a, along with the relative energies of B3LYP+IDSCRF/BS1 (see the Computational Details), from which one can observe that the relative energies and free energies calculated from the “mixed basis set” (BS1) are quite close to those emerging from the “medium-sized” DZVP all-electron one for most stationary points with some exceptions of multimetal-center structures (one Pd and two Ag atoms). The rate-determining step in the C–H activation process is the **INT-2** → **TS-3** → **INT-3** step, with an activation energy barrier of 16.7 (DZVP) or 14.4 (BS1) kcal/mol, easily surmounted at the elevated reaction temperature used (353 K). All other C–H activation steps proceed with lower energy barriers. The **INT-3** → **INT-4** proton transfer step should be noted, wherein **TS-4** is higher in energy than either of the two adjacent intermediates yet lower in free energy than both of the two intermediates.

The energy profiles for TM and RE processes are given in Figure 2b, from which one can observe that the formation of **INT-8** releases 6.9 kcal/mol energy for both calculation methods. In the following elementary TM and RE steps, the activation energy barriers are 11.1, 17.0, and 10.7 (DZVP) or 13.2, 18.0, and 15.4 (BS1) kcal/mol, respectively, and feasible under the experimental conditions used (353 K). It should be noted that the basis set effect is evident after **INT-11** since there involves the change of oxidation state from Pd(II) to Pd(0). In general, B3LYP+IDSCRF/BS1 predicts stronger interactions between coordinating ligands and Pd-center from shorter Pd–O or Pd–C bonds. As the decrease of coordination number, the structures of **TS-10** and **INT-12** become relatively less stable from B3LYP+IDSCRF/BS1 calculations. The oxidation process [**INT-12** + AgF + Ag(OAc)] → [**3a** + Pd(OAc)<sub>2</sub> + HF + Ag<sub>2</sub>] characterized with B3LYP+IDSCRF/DZVP is different from that of B3LYP+IDSCRF/BS1, and it seems quite thermodynamically favorable with the free energy change being −23.7 kcal/mol with B3LYP+IDSCRF/BS1 calculation. More detailed information is discussed in sections 2.2 and 2.3.

**2.2. Role of the AgF Additive.** The first role of AgF is to provide a source of HF to facilitate the TM process (Figure 3). Therein, a stable six-membered complex (**COM-a**) is formed, with a strong F···H–O H-bond resulting from the interaction of AgF and CH<sub>3</sub>COOH, with 25.8 kcal/mol energy being liberated through the combination of AgF + CH<sub>3</sub>COOH. As the O-atom in the CH<sub>3</sub>COOH hydroxyl group approaches the Ag center, the Ag–F bond is cleaved, forming complex **COM-b** via **TS1-HF**. Breaking of the F–H···O H-bond in **COM-b** is facilitated with the help of a dioxane solvent molecule, forming a HF···dioxane complex and Ag(OAc). The overall reaction releases 6.4 kcal/mol free energy, indicating that this process is both thermodynamically and kinetically accessible.

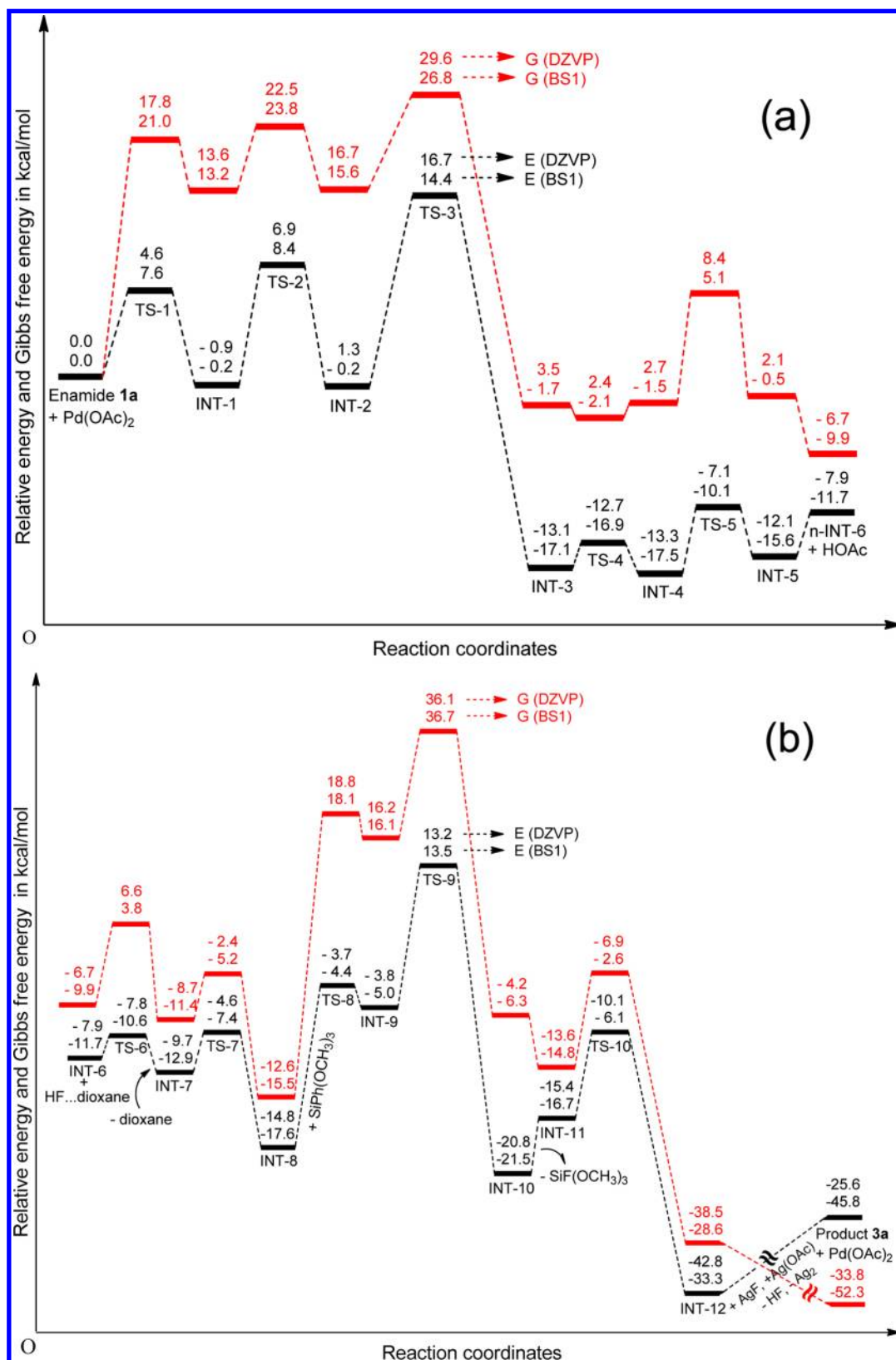
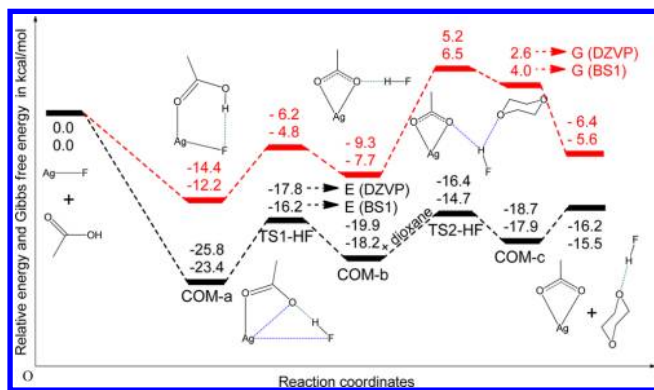


Figure 2. Relative energy and free energy profiles for the entire catalytic cycle: (a) C–H activation process; (b) TM, RE, and SP-RC process.

The second role of AgF is to recover the Pd(OAc)<sub>2</sub> catalyst with the help of Ag(OAc), itself formed from AgF + CH<sub>3</sub>COOH, in which 1 equiv each of AgF and Ag(OAc) salts are involved. The principal structure for the stationary points along the reaction pathways are depicted in Figure 4a,

along with values for the relative B3LYP/DZVP + SCRF energies and free energies. The interaction between INT-12 and AgF forms **COM-1**, a seven-membered ring structure with a Pd–Ag bond, with F...H and O–H distances of 1.30 and 1.10 Å, respectively. The hydrogen transfer from O to F proceeds

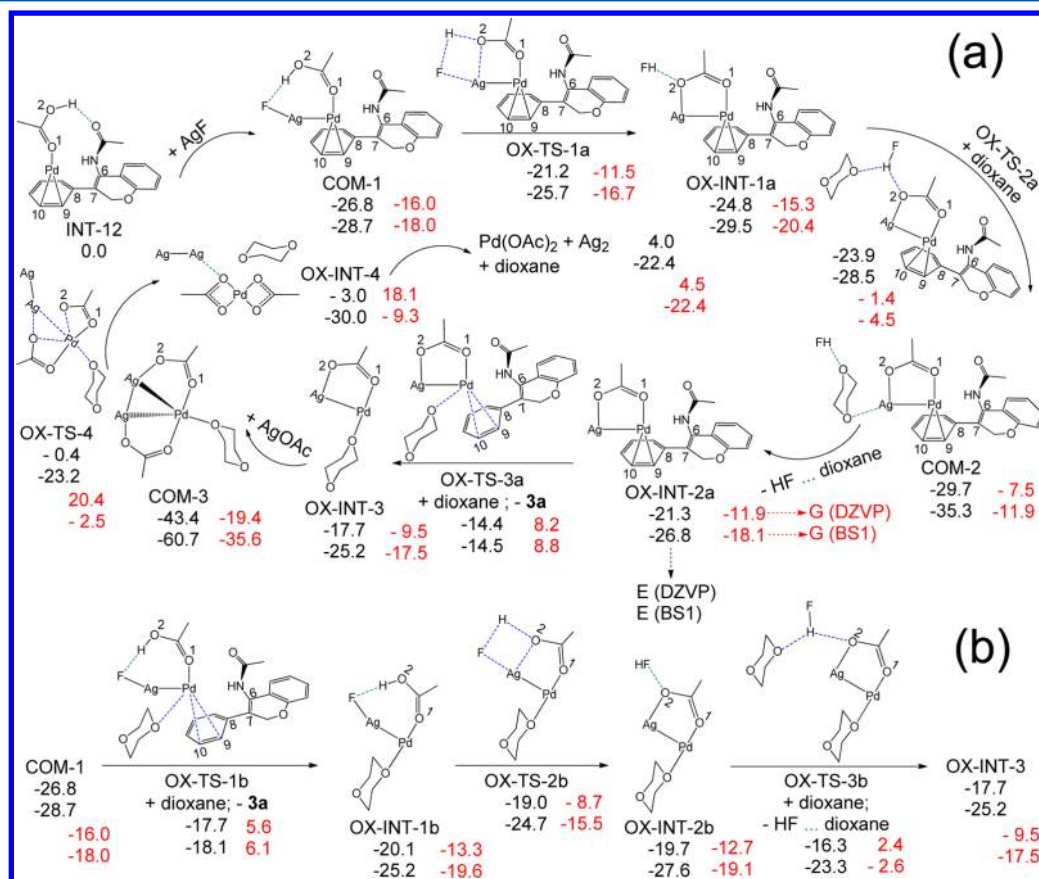


**Figure 3.** Relative energy and free energy profiles along the reaction pathway of  $\text{CH}_3\text{COOH} + \text{AgF} + \text{dioxane} \rightarrow \text{HF} \cdots \text{dioxane} + \text{Ag}(\eta^2\text{-OAc})$ , in which the partially formed or cleaved bonds in transition states and weak interatomic interactions are represented by dashed lines.

very easily via **OX-TS-1a**, in which the Ag–F bond is weakened and the O–Ag bond is formed. An intermediate (**OX-INT-1a**) is formed with a F–H $\cdots$ O H-bond, with the HF molecule pulled away from the O-atom with the assistance of a solvating dioxane via **OX-TS-2a** to form **COM-2**. This is followed by HF $\cdots$ dioxane leaving **COM-2** to form **OX-INT-2a**. Release of the product **3a** from **OX-INT-2a** is energetically challenging; however, a dioxane solvent molecules replaces **3a** in **OX-INT-2a** via **OX-TS-3a** to form **OX-INT-3**. The formal oxidation

state of Pd center in **OX-INT-3** is still zero, in which the linear or T-shaped structure is favorable for Pd(0). Attempts to fit an additional dioxane solvent molecule into the apparent vacant site of **OX-INT-3**, failed, as the structure shows the extra solvent sitting away from **OX-INT-3** (the Pd–O distance is  $\sim 3.01$  Å, normally it should be 2.20 Å). The introduction of a second Ag(OAc) salt molecule oxidizes Pd(0) center in **OX-INT-3** to Pd(II) in catalyst  $\text{Pd}(\text{OAc})_2$  via **OX-TS-4**, allowing recovery of the  $\text{Pd}(\text{OAc})_2$  catalyst concomitant with  $\text{Ag}_2$  and dioxane release. From the reaction profiles, one can see that the energy for most stationary points are well below those of **INT-12** +  $\text{AgF}$  +  $\text{AgOAc}$  + dioxane. The relative energies of the stationary points along the route [**OX-INT-3**  $\rightarrow$  **COM-3**  $\rightarrow$  **OX-TS-4**  $\rightarrow$  **OX-INT-4**  $\rightarrow$   $\text{Pd}(\text{OAc})_2$ ] are dependent on the basis sets employed, and these multiple- metal-center systems- (one Pd and two Ag atoms) have been predicted to be 17–27 kcal/mol more stable from the B3LYP+IDSCRF/BS1 calculations with respect to those emerging from the B3LYP +IDSCRF/DZVP calculations. This is related to the geometric parameters of Ag–Ag and Pd–Ag, for example, the distances of Ag–Ag and Pd–Ag in **COM-3** are 2.72 and 2.73 Å with B3LYP +IDSCRF/BS1, while they are 3.02 and 2.75 Å from B3LYP +IDSCRF/DZVP calculation.

Since the Ag-atom has a single-electron (i.e.,  $S = 1/2$ ), two Ag-atoms easily combine; calculations show a Ag–Ag bond dissociation energy in  $\text{Ag}_2$  to be  $\sim 31.9$  kcal/mol (i.e., Ag–Ag bonding is hard to be cleaved), close to the experimental measurement of 38.3 kcal/mol.<sup>15</sup> Hence, the oxidation process



**Figure 4.** Geometrical structures of all the stationary points involved in the solvent-assisted SP-RC process, along with their relative energies and free energies (kcal/mol), in which the partially formed or cleaved bonds in transition states and weak interatomic interactions are represented by dashed lines.



via the formation of  $\text{Ag}_2$  might be the favorable one. As the reaction proceeds,  $\text{Ag}_2$  might build up to form Ag metal (e.g., the free energy change of  $2\text{Ag}_2 \rightarrow \text{Ag}_4$  is  $-6.4$  kcal/mol), facilitating a forward shift in chemical equilibrium.

**2.3. Solvent Effect.** One potential mechanism to facilitate the oxidative conversion is that product **3a** separates from the ligand field prior to oxidation. However, direct separation of **3a** from **INT-12** is not feasible since this process increases the free energy by 7.4 kcal/mol, a thermodynamically prohibited process. This high energetic demand can be clearly understood through examination of the Pd–C bond lengths in this intermediate, ( $\sim 2.20$ – $2.30$  Å), which denote a strong Pd– $\pi$  interaction. There are two possibilities to eliminate **3a** from the Pd center. One involves a dioxane solvent molecule participating in the reaction, assisting separation of **3a** from the ligand field in **COM-1** via **OX-TS-1b** (Figure 4b). In **OX-TS-1b**, the Pd $\cdots$ O(dioxane) distance is 2.38 Å, similar to that in **OX-INT-1b**. Despite this, the Pd–C9 and Pd–C10 distances are 2.87 and 3.00 Å, respectively, about 0.57 and 0.77 Å longer than those in **COM-1**. The energy barrier for this process is only 9.1 kcal/mol, indicating that this step could easily proceed under the experimental condition employed (353K). In contrast, replacement of **3a** with dioxane could also occur at **OX-INT-2a** (Figure 4a), and involves an energy barrier of only 6.9 kcal/mol. Another role of the dioxane solvent is to eliminate HF from the strong F–H $\cdots$ O H-bond complex; see the **OX-INT-1a**  $\rightarrow$  **COM-2** (Figure 4a) or **OX-INT-2b**  $\rightarrow$  **OX-INT-3** (Figure 4b) transformations. However, solvent effect is quite complicated and involves a relatively large number of structural poses, combinations and permutations, each with significant influence on overall entropy contributions. Therefore, at present these are arguments for qualitative reference.

### 3. CONCLUSIONS

The B3LYP+IDSCRF/DZVP and B3LYP+IDSCRF/BS1 method has been employed in a series of DFT experiments to quantitatively characterize the geometric and energetic trends along the reaction path of a catalyzed combined C–H activation and C–C cross-coupling reaction. The following conclusions were reached: (1) The rate-determining step is the transmetalation step, with an activation energy of 21.1 kcal/mol, readily energetically accessible under the experimental conditions (353 K). (2) The role of  $\text{AgF}$  is 2-fold, including supplying HF to assist in the transmetalation reaction, while also helping in  $\text{Pd}(\text{OAc})_2$  catalyst recovery with the aid of  $\text{Ag}\cdots\text{Ag}$  and  $\text{Pd}\cdots\text{Ag}$  interactions. (3) The role of the dioxane solvent is to separate the product from the Pd ligand field while also assisting in the removal of HF from the strong F–H $\cdots$ O H-bond complex it forms, which could explain why the product yield is highly dependent on the solvent employed.

### 4. COMPUTATIONAL DETAILS

All minima and transition-state geometries were optimized and verified with the B3LYP method as implemented in Gaussian 09,<sup>16</sup> employing the standard double- $\zeta$  valence polarized (DZVP) all-electron basis set for all atoms.<sup>17</sup> The default self-consistent reaction field (SCRF) polarizable continuum model (PCM)<sup>18</sup> was used with dioxane as solvent (dielectric constant  $\epsilon = 2.2099$ ), while IDSCRF radii<sup>19</sup> were chosen as the atomic radii to define the molecular cavity, denoted B3LYP+IDSCRF. All resultant stationary points were subsequently characterized by vibrational analyses, from which their free energies were obtained for calculating the relative free energies, in addition to ensuring that the reactant, complex, intermediate, product, and transition-state structures resided at minima and first-order saddle

points, respectively, on their potential energy hypersurfaces. Intrinsic reaction coordinate (IRC)<sup>20a</sup> computations with the Hessian-based predictor–corrector integrator (HPC)<sup>20b,c</sup> were also used to trace selected reaction paths to confirm the optimized saddle point as being on the correct reaction pathway. All of optimized geometries have also been reoptimized and characterized with a mixed basis set(BS1) for comparison, in which the TZVP<sup>21</sup> basis set has been employed for H, C, N, O, F, and Si atoms and RSC 1997 ECP(SDD)<sup>22</sup> has been used for the Pd and Ag atoms.

## ■ ASSOCIATED CONTENT

### Supporting Information

Optimized geometric parameters for all stationary points; vibrational frequencies; total energy, zero-point energy, and total free energies; reaction mechanism and energy profile for transmetalation process without the assistance of HF molecule; complementary mechanistic characterizations for C–H activation. This material is available free of charge via the Internet at <http://pubs.acs.org>.

## ■ AUTHOR INFORMATION

### Corresponding Author

\*E-mail: dcfang@bnu.edu.cn.

### Notes

The authors declare no competing financial interest.

## ■ ACKNOWLEDGMENTS

This work was supported by the National Nature Science Foundation of China (21073016) and the Doctoral Program of Higher Education (20090003110008).

## ■ REFERENCES

- (1) Carey, F. A.; Sundberg, R. J. *Advanced Organic Chemistry*; Springer-Verlag: New York, 2007; Vol. A, pp 389–459.
- (2) (a) Miyaura, N.; Yamada, K.; Suzuki, A. *Tetrahedron Lett.* **1979**, 3437–3440. (b) Miyaura, N.; Yanagi, T.; Suzuki, A. *Synth. Commun.* **1981**, 11, 513–519. (c) Yin, J. J.; Rainka, M. P.; Zhang, X. X.; Buchwald, S. L. *J. Am. Chem. Soc.* **2002**, 124, 1162–1163. (d) Lysén, M.; Kristensen, J. L.; Vedsø, P.; Begtrup, M. *Org. Lett.* **2002**, 4, 257–259. (e) Selles, P.; Mueller, U. *Org. Lett.* **2004**, 6, 277–279.
- (3) (a) Kosugi, M.; Kurino, K.; Takayama, K.; Migita, T. *J. Organomet. Chem.* **1973**, 56, C11–C13. (b) Kosugi, M.; Shimizu, Y.; Migita, T. *Chem. Lett.* **1977**, 1423–1424. (c) Little, A. F.; Schwarz, L.; Fu, G. C. *J. Am. Chem. Soc.* **2002**, 124, 6343–6348. (d) Su, W. P.; Urgaonkar, S.; Verkade, J. G. *Org. Lett.* **2004**, 6, 1421–1424.
- (4) (a) Negishi, E. *Acc. Chem. Res.* **1982**, 15, 340–348. (b) Potter, G. A.; McCague, R. *J. Org. Chem.* **1990**, 55, 6184–6187. (c) Boudier, A.; Hupe, E.; Knochel, P. *Angew. Chem., Int. Ed.* **2000**, 39, 2294–2297. (d) Zhou, J.; Fu, G. C. *J. Am. Chem. Soc.* **2003**, 125, 12527–12530.
- (5) (a) Hiyama, T. *J. Organomet. Chem.* **2002**, 653, 58–61. (b) Marciniak, B.; Majchrzak, M.; Prukala, W.; Kubicki, M.; Chadyniak, D. *J. Org. Chem.* **2005**, 70, 8550–8555. (c) Srimani, D.; Sawoo, S.; Sarkar, A. *Org. Lett.* **2007**, 9, 3639–3642. (d) Raders, S. M.; Kingston, J. V.; Verkade, J. G. *J. Org. Chem.* **2010**, 75, 1744–1747. (e) Srimani, D.; Bej, A.; Sarkar, A. *J. Org. Chem.* **2010**, 75, 4296–4299.
- (6) Chen, X.; Engle, K. M.; Wang, D. H.; Yu, J. Q. *Angew. Chem., Int. Ed.* **2009**, 48, 5094–5115.
- (7) (a) Wu, J. L.; Cui, X. L.; Chen, L. M.; Jiang, G. J.; Wu, Y. J. *J. Am. Chem. Soc.* **2009**, 131, 13888–13889. (b) Rosewall, C. F.; Sibbald, P. A.; Liskin, D. V.; Michael, F. E. *J. Am. Chem. Soc.* **2009**, 131, 9488–9489. (c) Benfatti, F.; Capdevila, M. G.; Zoli, L.; Benedetto, E.; Cozzi, P. G. *Chem. Commun.* **2009**, 5919–5921. (d) Chaumontet, M.; Retailleau, P.; Baudoin, O. *J. Org. Chem.* **2009**, 74, 1774–1776. (e) Kumar, R. K.; Ali, M. A.; Punniyamurthy, T. *Org. Lett.* **2011**, 13, 2102–2105. (f) Thu, H. Y.; Yu, W. Y.; Che, C. M. *J. Am. Chem. Soc.* **2006**, 128, 9048–9049. (g) Wang, X. S.; Lu, Y.; Dai, H. X.; Yu, J. Q. *J.*

- Am. Chem. Soc.* **2010**, *132*, 12203–12205. (h) Lu, Y.; Wang, D. H.; Engle, K. M.; Yu, J. Q. *J. Am. Chem. Soc.* **2010**, *132*, 5916–5921. (i) Kesharwani, T.; Larock, R. C. *Tetrahedron* **2008**, *64*, 6090–6102. (j) Song, G. Y.; Wang, F.; Li, X. W. *Chem. Soc. Rev.* **2012**, *41*, 3651–3678. (k) Giri, R.; Shi, B. F.; Engle, K. M.; Maugel, N.; Yu, J. Q. *Chem. Soc. Rev.* **2009**, *38*, 3242–3272. (l) Lersch, M.; Tilset, M. *Chem. Rev.* **2005**, *105*, 2471–2526. (m) Cunay, A.; Theopold, K. H. *Chem. Rev.* **2010**, *110*, 1060–1081. (n) Whisler, M. C.; MacNeil, S.; Snieckus, V.; Beak, P. *Angew. Chem., Int. Ed.* **2004**, *43*, 2206–2225.
- (8) (a) Chen, X.; Goodhue, C. E.; Yu, J. Q. *J. Am. Chem. Soc.* **2006**, *128*, 12634–12635. (b) Giri, R.; Maugel, N.; Li, J. J.; Wang, D. H.; Breazzano, S. P.; Saunders, L. B.; Yu, J. Q. *J. Am. Chem. Soc.* **2007**, *129*, 3510–3511. (c) Chu, J. H.; Chen, C. C.; Wu, M. J. *Organometallics* **2008**, *27*, 5173–5176. (d) Zhou, H.; Chung, W. J.; Xu, Y. H.; Loh, T. P. *Chem. Commun.* **2009**, 3472–3474. (e) Ge, H.; Niphakis, M. J.; Georg, G. I. *J. Am. Chem. Soc.* **2008**, *130*, 3708–3709. (f) Wang, D. H.; Mei, T. S.; Yu, J. Q. *J. Am. Chem. Soc.* **2008**, *130*, 17676–17677. (g) Mkhaliid, I. A.; Barnard, J. H.; Marder, T. B.; Murphy, J. M.; Hartwig, J. F. *Chem. Rev.* **2010**, *110*, 890–931. (h) Hartwig, J. F. *Chem. Soc. Rev.* **2011**, No. 40, 1992–2002.
- (9) (a) Chen, X.; Li, J. J.; Hao, X. S.; Goodhue, C. E.; Yu, J. Q. *J. Am. Chem. Soc.* **2006**, *128*, 78–79. (b) Kawai, H.; Kobayashi, Y.; Qi, S. C.; Inoue, Y. *Chem. Commun.* **2008**, 1464–1466.
- (10) (a) Sezen, B.; Franz, R.; Sames, D. *J. Am. Chem. Soc.* **2002**, *124*, 13372–13373. (b) Yang, S. D.; Li, B. J.; Wan, X. B.; Shi, Z. J. *J. Am. Chem. Soc.* **2007**, *129*, 6066–6067. (c) Zhou, H.; Xu, Y. H.; Chung, W. J.; Loh, T. P. *Angew. Chem., Int. Ed.* **2009**, *48*, 5355–5357.
- (11) (a) Yoshikai, N.; Matsumoto, A.; Norinder, J.; Nakamura, E. *Angew. Chem., Int. Ed.* **2009**, *48*, 2925–2928. (b) Norinder, J.; Matsumoto, A.; Yoshikai, N.; Nakamura, E. *J. Am. Chem. Soc.* **2008**, *130*, 5858–5859.
- (12) (a) Jensen, M. P.; Wick, D. D.; Reinartz, S.; White, P. S.; Templeton, J. L.; Goldberg, K. I. *J. Am. Chem. Soc.* **2003**, *125*, 8614–8624. (b) Lafrance, M.; Rowley, C. N.; Woo, T. K.; Fagnou, K. J. *J. Am. Chem. Soc.* **2006**, *128*, 8754–8756. (c) Garcia-Cuadrado, D.; Mendoza, P. De; Braga, A. A. C.; Maseras, F.; Echavarren, A. M. *J. Am. Chem. Soc.* **2007**, *129*, 6880–6886. (d) Li, L.; William, W.; Jones, W. D. *Organometallics* **2009**, *28*, 3492–3500. (e) Walstrom, A.; Pink, M.; Tsvetkov, N. P.; Fan, H.; Ingleson, M.; Caulton, K. G. *J. Am. Chem. Soc.* **2005**, *127*, 16780–16781. (f) Asplund, M. C.; Snee, P. T.; Yeston, J. S.; Willkens, M. J.; Payne, C. K.; Yang, H.; Kotz, K. T.; Frei, H.; Bergman, R. G.; Harris, C. B. *J. Am. Chem. Soc.* **2002**, *124*, 10605–10612. (g) Su, M. D.; Chu, S. Y. *Chem.—Eur. J.* **1999**, *5*, 198. (h) Reinhold, M.; McGrady, J. E.; Perutz, R. N. *J. Am. Chem. Soc.* **2004**, *126*, 5268–5276. (i) Yang, X. Z.; Hall, M. B. *J. Phys. Chem. A* **2009**, *113*, 2152–2157. (j) Maron, L.; Eisenstein, O. *J. Am. Chem. Soc.* **2001**, *123*, 1036–1039. (k) Davies, D. L.; Donald, S. M. A.; Macgregor, S. A. *J. Am. Chem. Soc.* **2005**, *127*, 13754–13755. (l) Pascual, S.; Mendoza, P. de; Braga, A. A. C.; Maseras, F.; Echavarren, A. M. *Tetrahedron* **2008**, *64*, 6021–6029. (m) Balcells, D.; Clot, E.; Eisenstein, O. *Chem. Rev.* **2010**, *110*, 749–823.
- (13) (a) Miyaura, N. *J. Organomet. Chem.* **2002**, *653*, 54–57. (b) Hiyama, T. *J. Organomet. Chem.* **2002**, *653*, 58–61. (c) Hatanaka, Y.; Hiyama, T. *J. Org. Chem.* **1988**, *53*, 918–920. (d) Braga, A. A. C.; Morgon, N. H.; Ujaque, G.; Maseras, F. *J. Am. Chem. Soc.* **2005**, *127*, 9298–9307. (e) Sugiyama, A.; Ohnishi, Y.; Nakaoka, M.; Nakao, Y.; Sato, H.; Sakaki, S.; Nakao, Y.; Hiyama, T. *J. Am. Chem. Soc.* **2008**, *130*, 12975–12985.
- (14) (a) Ananikov, V. P.; Musaev, D. G.; Morokuma, K. *Eur. J. Inorg. Chem.* **2007**, 5390–5399. (b) Pérez-Rodríguez, M.; Braga, A. A. C.; Garcia-Melchor, M.; Pérez-Temprano, M. H.; Casares, J. A.; Ujaque, G.; de Lera, A. R.; Alvarez, R.; Maseras, F.; Espinet, P. *J. Am. Chem. Soc.* **2009**, *131*, 3650–3657.
- (15) Huber, K. P.; Herzberg, G. *Molecular Spectra and Molecular Structure I*; Van Nostrand Reinhold: New York, 1950.
- (16) Frisch, M. J.; Trucks, G. W.; Schlegel, H. B.; Scuseria, G. E.; Robb, M. A.; Cheeseman, J. R.; Scalmani, G.; Barone, V.; Mennucci, B.; Petersson, G. A.; Nakatsuji, H.; Caricato, M.; Li, X.; Hratchian, H. P.; Izmaylov, A. F.; Bloino, J.; Zheng, G.; Sonnenberg, J. L.; Hada, M.; Ehara, M.; Toyota, K.; Fukuda, R.; Hasegawa, J.; Ishida, M.; Nakajima, T.; Honda, Y.; Kitao, O.; Nakai, H.; Vreven, T.; Montgomery, J. A., Jr.; Peralta, J. E.; Ogliaro, F.; Bearpark, M.; Heyd, J. J.; Brothers, E.; Kudin, K. N.; Staroverov, V. N.; Kobayashi, R.; Normand, J.; Raghavachari, K.; Rendell, A.; Burant, J. C.; Iyengar, S. S.; Tomasi, J.; Cossi, M.; Rega, N.; Millam, J. M.; Klene, M.; Knox, J. E.; Cross, J. B.; Bakken, V.; Adamo, C.; Jaramillo, J.; Gomperts, R.; Stratmann, R. E.; Yazyev, O.; Austin, A. J.; Cammi, R.; Pomelli, C.; Ochterski, J. W.; Martin, R. L.; Morokuma, K.; Zakrzewski, V. G.; Voth, G. A.; Salvador, P.; Dannenberg, J. J.; Dapprich, S.; Daniels, A. D.; Farkas, O.; Foresman, J. B.; Ortiz, J. V.; Cioslowski, J.; Fox, D. J. *Gaussian 09, Revision A.02*, Gaussian, Inc., Wallingford, CT, 2009.
- (17) (a) Godbout, N.; Salahub, D. R.; Andzelm, J.; Wimmer, E. *Can. J. Chem.* **1992**, *70*, 560–571. (b) Sosa, C.; Lee, C. J. *J. Phys. Chem.* **1992**, *96*, 6630–6636.
- (18) Scalmani, G.; Frisch, M. J. *J. Chem. Phys.* **2010**, *132*, 114110–114124.
- (19) (a) Tao, G. Y.; Mu, W. H.; Chass, G. A.; Tang, T.-H.; Fang, D.-C. *Int. J. Quantum Chem.* **2013**, *113*, 975–984. (b) Fang, D.-C. *SCRF-RADII*; Beijing Normal University: Beijing, China, free of charge for academic users.
- (20) (a) Fukui, K. *Acc. Chem. Res.* **1981**, *14*, 363–368. (b) Hratchian, H. P.; Schlegel, H. B. *J. Chem. Phys.* **2004**, *120*, 9918–9924. (c) Hratchian, H. P.; Schlegel, H. B. *J. Chem. Theor. Comput.* **2005**, *1*, 61–69.
- (21) Schaefer, A.; Huber, C.; Ahlrichs, R. *J. Chem. Phys.* **1994**, *100*, 5829–5835.
- (22) Andrae, D.; Haeussermann, U.; Dolg, M.; Stoll, H.; Preuss, H. *Theor. Chim. Acta* **1990**, *77*, 123–141.